J Mater Sci (2008) 43:6038–6048
DOI 10.1007/s10853-008-2955-9

Detailed investigation of ultrasonic Al–Cu wire-bonds: II. Microstructural evolution during annealing

M. Drozdov · G. Gur · Z. Atzmon · W. D. Kaplan

Received: 9 July 2008 / Accepted: 14 August 2008 / Published online: 4 September 2008

Abstract Scanning and transmission electron microscopy were used to study the interface composition and morphology of copper wire-bonds heat-treated at 175 °C for 2, 24, 96, and 200 h in argon. Detailed morphological and compositional characterization of the Al–Cu heat-treated interfaces was conducted on site-specific specimens prepared by focused ion beam milling. Discontinuous intermetallic grains with varying size and morphology were found to grow in regions where they originally nucleated during the bonding process. The main intermetallic phase was Al_2Cu, which was found to grow via solid-state diffusion. In specimens heat-treated for 96 and 200 h, the Al_4Cu_9 phase was also detected. Void formation at the Al–Cu bonds heat-treated up to 200 h was not found to be a source of bond failure.

Introduction

Wire bonding is one of the main technologies used to perform electronic\chip interconnection. During the wire bonding process, combined mechanical, ultrasonic, and thermal energies are applied to ensure an intimate connection between the wire and the IC pad [1]. More detailed explanations regarding the wire-bonding process are provided in a companion paper [2].

It should be noted that while the presence of intermetallic phases indicates that an intimate contact occurred at the interface, it is not an obligatory condition for bonding. Bonding means physical–chemical bonds form at the interface, which is facilitated by charge transfer. Therefore bonding can occur between two completely immiscible solids without the formation of secondary phases. For example, charge transfer at metal–oxide interfaces results in a measurable mechanical work of adhesion without the formation of intermediate phases at the interface [3, 4]. However, Al–Cu intermetallic evolution during aging of wire-bonds can significantly influence bond reliability, and it is an important topic for research for wire-bonding applications.

Gold wires are typically used in advanced wire-bonding processes. However, copper wires are currently being evaluated as a substitute for gold due to reduced cost, superior thermal and electrical conductivity, and higher metallurgical stability. Very little quantitative information regarding the aging of Al–Cu wire-bonds is available. This, together with the lack of accepted quality assurance methods, inhibits the incorporation of copper wires into commercial devices. The available morphological and compositional data regarding the aging of Al–Cu wire-bonds is inaccurate and incomplete, since the methods currently used to analyze Al–Cu wire-bonds have insufficient resolution for detailed interface analysis. In order to obtain reliable data regarding the evolution of the wire-bonded interfaces, the use of transmission electron microscopy (TEM) is required [5–15].

In this research, annealed wire-bonded interfaces were characterized by TEM, energy dispersive spectroscopy (EDS) mounted on a TEM, and selected area diffraction

M. Drozdov · W. D. Kaplan (✉)
Department of Materials Engineering, Technion—Israel Institute of Technology, Haifa 32000, Israel
e-mail: kaplan@tx.technion.ac.il

G. Gur · Z. Atzmon
Kulicke & Soffa Bonding Tools, Yokneam Elite, Israel

(SAD) analysis, while site-specific and relatively artifact-free specimen preparation was conducted using a dual-beam focused ion beam (FIB). In order to obtain information on time-dependent evolution of the wire-bonded Al–Cu interfaces, the Al–Cu wire-bonds were heat-treated at 175 °C for 2, 24, 96, and 200 h. The morphology and composition of *as-bonded* Al–Cu wire-bonds is discussed in a companion paper [2].

Experimental methods

Specimen preparation

Copper wires were bonded on top of Si wafers coated with thermally grown SiO_2 and covered by uniform Al metallization. The Al metallization consisted of 0.5 wt.% Cu and 1 wt.% Si. The copper wire that was used for the bonding was 25.4 μm in diameter and 99.99% pure (4 N). Ball bonding was performed on a Kulicke & Soffa Model 8028PPS Automatic Wire Bonder using a capillary with an inner chamfer of 90° (IC 90). The ball bond diameter was kept within 52 ± 3 μm. Thermosonic ball bonding of each Si die was performed at 220 °C for an approximate time of 18 s per device (<0.2 s per bond) with a pre-heat and post-heat of 18 s at 150 °C. The bonding parameters were optimized to ensure zero pad peals, which is an essential condition for successful copper wire-bonding, and the resulting average bond shear force was 13.3 kg/mm^2, which corresponds to an optimal shear strength of as-bonded Al–Au wire-bonds [16]. In order to ensure uniform and symmetric bonds, free air balls at the Cu wire tip were formed by melting the tips of the Cu wires in a reducing atmosphere (95%N_2, 5%H_2) prior to the bonding stage.

Devices may be subjected to elevated temperatures during their life spans. It is currently accepted that the maximum temperature that a wire-bond is expected to withstand is 175 °C. Therefore, to investigate time-dependent accelerated aging of the Al–Cu wire-bonds, devices were heat-treated at 175 °C for 2, 24, 96, and 200 h. In order to simulate encapsulation in a nominally inert adhesive, the specimens were heat-treated in argon, in sealed Pyrex tubes, which were evacuated to a vacuum of 5×10^{-1} torr and filled with 99.999% pure argon. This vacuum-flush procedure was repeated three times before the tubes were hermetically sealed. In order to obtain a complete analysis of the bonded interface, the central and peripheral regions of each wire-bonded specimen were examined.

TEM specimens were prepared using the "in situ lift-out" method in a dual-beam FIB [14, 15, 17]. Specimen characterization during the TEM specimen preparation process was conducted using the scanning electron microscopy (SEM) mode of a dual-beam FIB. At the final stages of TEM specimen preparation, scanning TEM (STEM) in the FIB was used to monitor specimen thickness. During SEM and TEM specimen preparation in the FIB, 30 kV gallium ions were oriented perpendicular to the Al–Cu interface to minimize beam damage of the TEM specimen. A specimen cleaning routine was executed at 5 kV at an incident angle of 5–7° to the TEM specimen [14].

Characterization

As initial characterization of the copper bonds was conducted using secondary electrons (SE) in SEM mode of the dual-beam FIB, an immersed-lens mode of SE acquisition was used for better spatial resolution. STEM, mounted on the dual-beam FIB, was used for initial characterization of the TEM specimens. This provided qualitative information on the thickness of the TEM specimens during thinning and initial morphological characterization of the specimens.

Extensive morphological characterization of the Al–Cu bonds was conducted using TEM on a number of different instruments: JEOL 3010UHR (ultra high resolution) TEM, FEI Tecnai G^2 F20 field emission gun-TEM with a high-angle annular dark field (HAADF) STEM detector and a retractable EDAX detector, and an FEI Tecnai G^2 20 with a retractable EDAX detector. The Al–Cu intermetallic grain size was measured from STEM micrographs.

TEM specimens were prepared both from central and peripheral regions of the annealed bonds. The "central" and "peripheral" regions relate to a region located within 10 μm from the center of the bond, or 10 μm from the edge of a bond, respectively.

Compositional analysis

In order to obtain information regarding the Al–Cu interface composition, heat-treated interfaces were studied using EDS, with SAD used to confirm the crystal structure of the phases. EDS analysis was conducted using FEI Tecnai F20 and Tecnai T20 microscopes, following the standardless procedure. In order to ensure acquisition of the signal from a selected region, the specimen was tilted 15° towards the EDS detector. The nominal beam diameters used for EDS analysis in the Tecnai F20 and Tecnai T20 were 0.65 and 1.6 nm, respectively.

SAD patterns were acquired from the intermetallic grains found adjacent to the interface region, which were also characterized by TEM-EDS. The diffraction patterns were acquired using the Tecnai T20 TEM and JEOL 3010 UHR TEM.

Results

Specimens heat-treated in argon for 2 h at 175 °C

Figure 1 presents a high-resolution (HR) SEM micrograph acquired from the periphery of a specimen heat-treated for 2 h in argon. Discontinuous intermetallics can be detected at the Al–Cu interface. Voids can also be found at the Al–Cu interface. Pores in the copper ball are indicated.

A HRSEM micrograph, acquired from the center of a bond heat-treated for 2 h in argon, is presented in Fig. 2. A continuous layer of small, relatively uniform, intermetallic grains are visible at the Al–Cu interface. Pores in the copper ball are also visible. No voids are present at the Al–Cu interface.

Figure 3 presents a HAADF STEM micrograph of a specimen prepared from the peripheral region of a wire-bond heat-treated for 2 h in argon. Discontinuous intermetallic regions are visible at the Al–Cu interface. A distorted intermetallic region, similar to the one found at the periphery of the as-bonded specimen [2], is visible at the Al–Cu interface on the right side of the micrograph. The change of copper concentration over this region is not uniform. Grains with a low copper concentration are located near the copper ball, together with copper-rich grains located closer to the aluminum layer. In the distorted region, intermetallic grains with a copper concentration of up to 50 at.% can be identified. Regions with a higher copper concentration, including a solid solution of aluminum in copper (noted as α-Cu), are also detectable at the Al–Cu interface. Some voids are also present at the interface. The copper grains located just above the distorted region are significantly smaller than those located further away from the distorted region (Table 1).

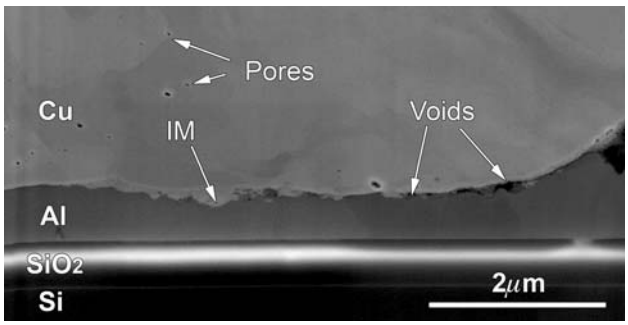

Fig. 1 SE HRSEM micrograph acquired from the periphery of a copper wire-bond heat-treated for 2 h at 175 °C in argon

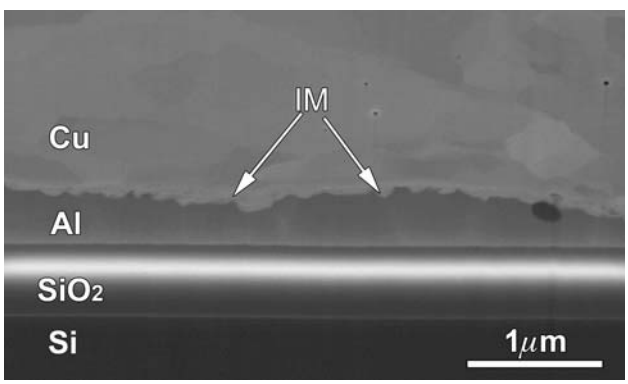

Fig. 2 SE HRSEM micrograph acquired from the central region of a copper wire-bond heat-treated for 2 h at 175 °C in argon

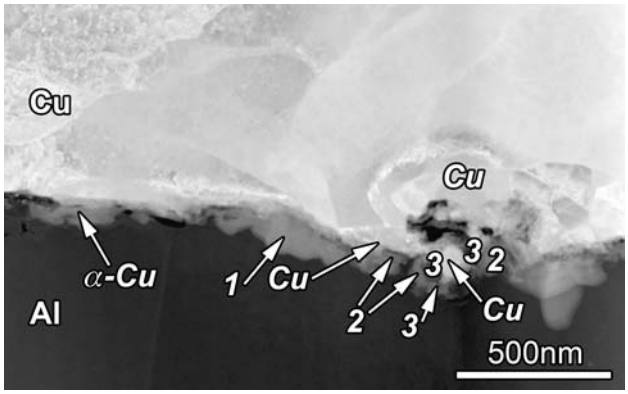

Fig. 3 HAADF-STEM micrograph of the peripheral region of a wire-bond heat-treated at 175 °C for 2 h in argon. The STEM-EDS results of the annotated regions are presented in Table 1

Table 1 The Cu to Al concentration ratios, as measured by STEM-EDS from the regions noted in Fig. 3

	Cu (at.%, relative to Al) (%)
Region 1	59 ± 2
Regions marked as 2	42.4 ± 4
Regions marked as 3	30.1 ± 2.6

In the micrograph acquired from the central region of a bond heat-treated for 2 h in argon (Fig. 4), more uniform intermetallic grains are present. The coverage of the Al–Cu interface by the intermetallics is also more complete. The copper concentration (measured by STEM-EDS) of the intermetallic grains varied between 26 and 44 at.% Cu (relative to Al), while the composition of the grains marked as 2 and 4 are close to that of the Al_2Cu phase (θ). The SAD patterns from grains 1 and 4 confirmed the presence of the Al_2Cu phase. A grain with dark contrast, noted on the micrograph by a black arrow, contains 7 wt.% Cu, while three aluminum grains adjacent to it contain no more than 1 wt.% Cu (Table 2).

Specimens heat-treated in argon for 24 h at 175 °C

HRSEM micrographs of the central and peripheral regions of the wire-bond, heat-treated for 24 h in argon, are

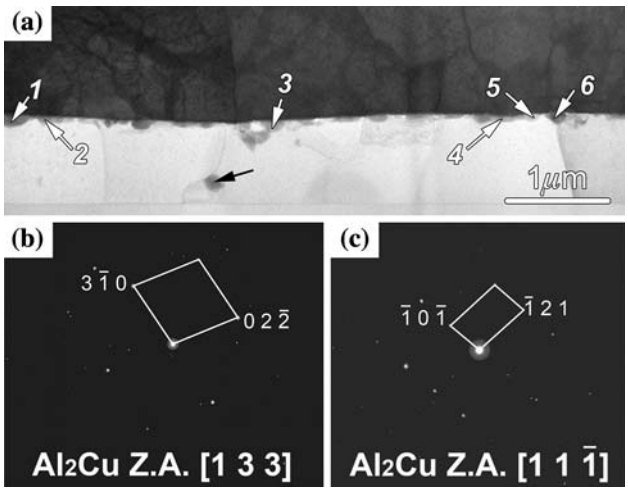

Fig. 4 (**a**) BF STEM micrograph of the central region of a wire-bond heat-treated at 175 °C for 2 h in argon. (**b**, **c**) Present SAD patterns of the grain annotated as 1 and 4 on the STEM micrograph. The STEM-EDS results of grains 1–6 are presented in Table 2

Table 2 The Cu to Al concentration ratios, as measured by STEM-EDS from the regions noted in Fig. 4

Grains	Cu (at.%, relative to Al) (%)
1	40.2 ± 1.3
2 and 4	33.2 ± 2.3
3	41.5 ± 1
5	26.9 ± 0.6
6	43.3 ± 1.2

presented in Fig. 5. The intermetallic coverage of the Al–Cu interface is discontinuous. The intermetallics found at the bond center are more uniform and continuous (Fig. 5a), while the intermetallics found at the bond periphery are discontinuous and less uniform (Fig. 5b). The aluminum metallization is thinner in regions of intermetallic growth at both the bond center and the bond periphery.

Figure 6 presents a bright field (BF) STEM micrograph taken from the peripheral region of a wire-bond heat-treated for 24 h in argon. The coverage of the Al–Cu interface by intermetallic grains is discontinuous. The shape of the grains is not uniform; smaller grains located adjacent to the copper region can be found together with larger grains. The composition of intermetallic grains and regions that are annotated on the micrographs measured by STEM-EDS are presented in Table 3. The majority of large intermetallic grains (noted as 3, 4, and 6) have a composition (within the error) matching that of the Al_2Cu phase. In regions adjacent to the copper ball, intermetallics with higher copper concentrations can be found. The oxidized region, located near the copper ball, was identified by STEM-EDS and SAD as CuO. Analysis of the SAD patterns, acquired from the grains indicated as 2 and 4, confirmed the presence of the Al_2Cu phase. Grain 3 was identified by SAD as Al_2Cu_3.

Figure 7 is a BF STEM micrograph taken from the center of a bond heat-treated for 24 h in argon. The large holes at the center of the micrograph were introduced during TEM specimen preparation. The intermetallic coverage of the central region of the bond is more complete than that of the peripheral region of the bond (as shown in Fig. 6). The composition of the majority of large intermetallic grains (noted as 1, 4, and 8), as measured by STEM-EDS, is close to that of the Al_2Cu phase. Smaller intermetallic regions, adjacent to the copper layer, were identified by STEM-EDS as regions of higher copper concentration. SAD patterns, acquired from the grains indicated on the micrograph by 4 and 5, confirmed the presence of the Al_2Cu phase (Table 4).

Specimens heat-treated in argon for 96 h at 175 °C

Figure 8 presents HRSEM micrographs of the peripheral and central regions of a wire-bond heat-treated for 96 h in argon. The intermetallic coverage of the Al–Cu interface is discontinuous, with fewer intermetallic grains found in the periphery of the bond than at the center. Voids between the intermetallics and the copper wire were found at the bond periphery.

A BF STEM micrograph, taken from the periphery of a bond heat-treated for 96 h in argon, is presented in Fig. 9a. The large voids visible in the micrograph were expanded by ion milling during the specimen preparation process. A discontinuous intermetallic layer is visible in Fig. 9a.

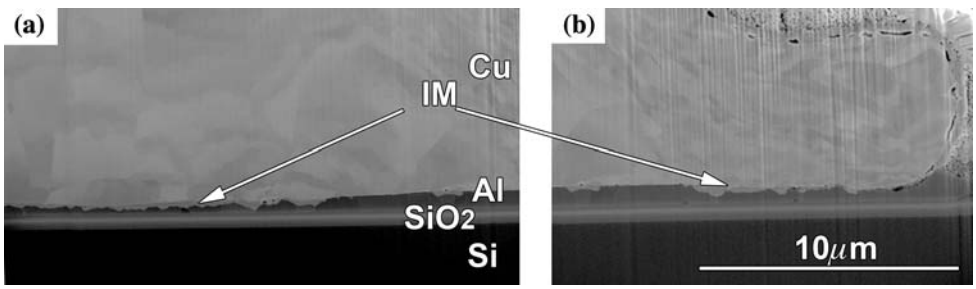

Fig. 5 SE HRSEM micrographs of (**a**) the center and (**b**) the periphery of a copper wire-bond heat-treated for 24 h at 175 °C in argon. A discontinuous intermetallic layer is detected. The scale bar is equivalent for both micrographs

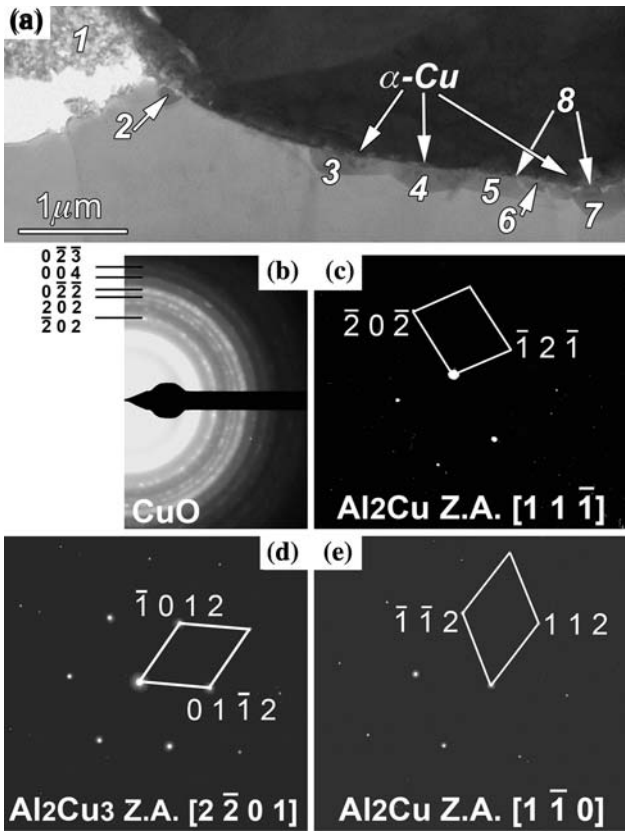

Fig. 6 (**a**) BF STEM micrograph of the peripheral region of a wire-bond heat-treated at 175 °C for 24 h in argon. (**b**) SAD diffraction ring acquired from a region noted as 1 on the STEM micrograph. (**c**–**e**) SAD patterns taken from grains noted as 2–4, respectively. The STEM-EDS results from the annotated regions are provided in Table 3

Table 3 The Cu to Al concentration ratios, as measured by STEM-EDS from the regions noted in Fig. 6

	Cu (at.%, relative to Al) (%)
Grain 2	37.7 ± 2.7
Grain 3	34.8 ± 3.8
Grain 4	36.3 ± 5.6
Grain 5	18.2 ± 1.7
Grain 6	33.9 ± 0.6
Grain 7	46.5 ± 3
Region 8	73.1 ± 5

Region 1 was found by EDS to match the CuO phase, with an error of 7 at.%

Intermetallics of with two different contrasts can be distinguished; large intermetallic grains with a brighter contrast and smaller intermetallic regions with a darker contrast located between the copper ball and the large intermetallic grains. The composition of the large intermetallic grains, noted as 1–5, 8, and 9, is close to the composition of the Al_2Cu phase (within 4 at.%). SAD

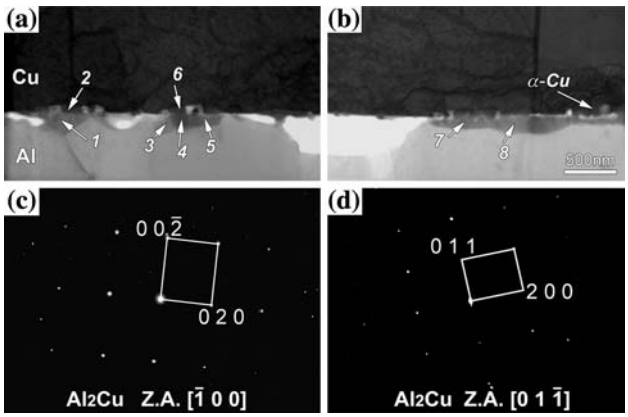

Fig. 7 (**a**, **b**) BF STEM micrographs of the central region of a wire-bond heat-treated at 175 °C for 24 h in argon. The scale bar is equivalent for both micrographs. (**b**, **c**) SAD patterns taken from grains noted as 4 and 5, respectively. The STEM-EDS results of the annotated regions are indicated in Table 4

Table 4 The Cu to Al concentration ratios, as measured by STEM-EDS from the grains noted in Fig. 7

Grain	Cu (at.%, relative to Al) (%)
1	35.5 ± 0.6
2	73.5 ± 0.7
3	22.7 ± 3.5
4	37.7 ± 0.8
5	34.3 ± 0.8
6	65.2 ± 1.1
7	38.3 ± 1
8	32.1 ± 0.7

patterns confirmed the presence of Al_2Cu in the large grains indicated on the micrograph as 1, 2, 8, and 9. Smaller intermetallic regions with a darker contrast were found by STEM-EDS to contain a larger atomic percent of copper (between 45 and 70 at.% Cu). The presence of Al_4Cu_9 in the smaller intermetallic grains, noted on the micrograph as 10 and 12, was confirmed by SAD patterns. Voids found at the Al–Cu interface are located mainly between the copper ball and the intermetallics, and between the two intermetallic phases (Table 5).

Figure 10 presents a BF STEM micrograph acquired from the center of a bond heat-treated for 96 h in argon. Two continuous intermetallic layers are distinguishable; a thinner layer with a darker contrast adjacent to the copper region, and a thicker layer consisting of larger and relatively uniform-shaped grains with a brighter contrast. The large intermetallic grains were found by STEM-EDS to contain 37–40 at.% Cu. The darker intermetallic layer was found to contain >70 wt.% Cu. The SAD patterns acquired from the large grains indicated on the micrograph by 1–3 and 5, confirmed the presence of Al_2Cu (Table 6).

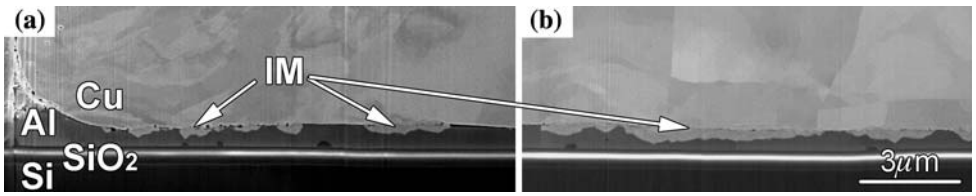

Fig. 8 SE HRSEM micrographs of (**a**) the periphery and (**b**) the center of a copper wire-bond heat-treated for 96 h at 175 °C in argon. A discontinuous intermetallic layer is detected. The scale bar is equivalent for both micrographs

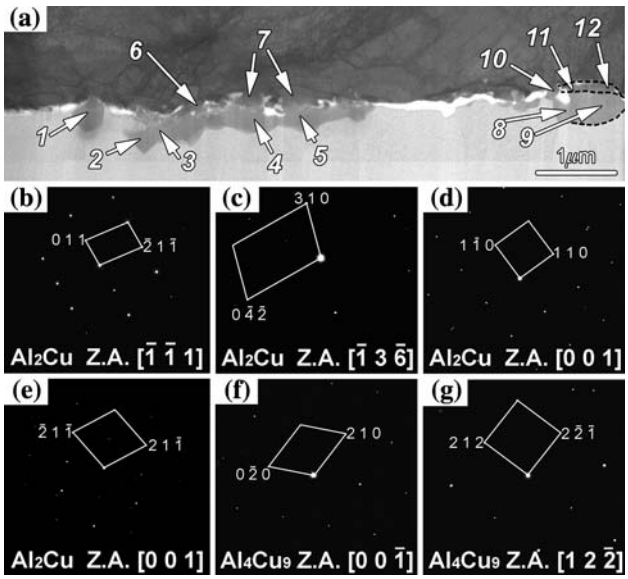

Fig. 9 (**a**) BF STEM micrograph of the peripheral region of a wire-bond heat-treated at 175 °C for 96 h in argon. Two discontinuous intermetallic layers of with different contrast and shapes are marked by dashed lines. (**b**–**g**) SAD patterns from grains indicated as 1, 2, 8–10, and 12, respectively. The STEM-EDS results of the annotated grains are presented in Table 5

Table 5 The Cu to Al concentration ratios, as measured by STEM-EDS from the regions noted in Fig. 9

	Cu (at. %, relative to Al) (%)
Grain 1	36.1 ± 2.6
Grain 2	34 ± 0.7
Grain 3	33.7 ± 1.2
Grain 4	33.5 ± 1.1
Grain 5	33.6 ± 1.5
Grain 6	67.1 ± 2.1
Region 7	71.5 ± 8
Grain 8	36.9 ± 1.2
Grain 9	36 ± 1.3
Grain 10	46.3 ± 7.3
Grain 11	53.7 ± 0.8
Grain 12	68.9 ± 0.7

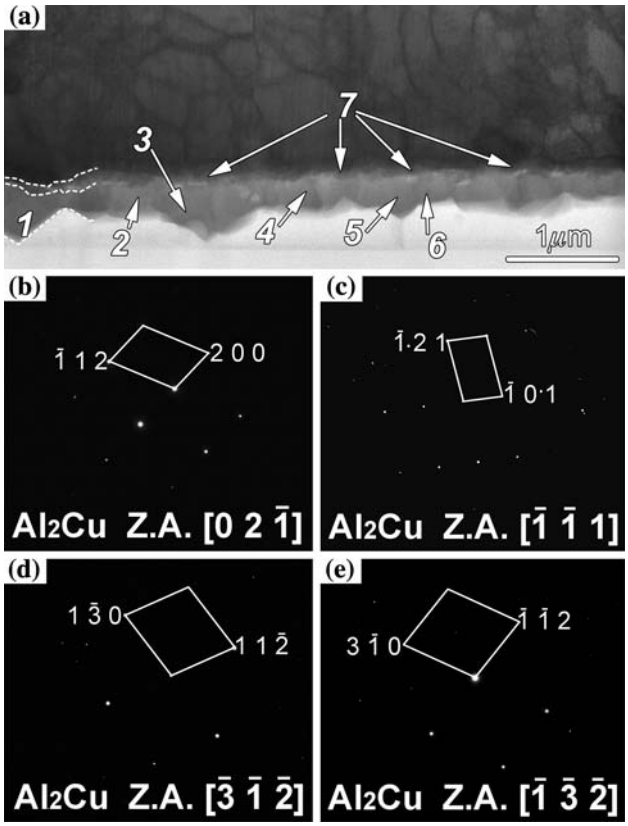

Fig. 10 (**a**) BF STEM micrograph of the central region of a wire-bond heat-treated at 175 °C for 96 h in argon. Two continuous intermetallic layers of different contrasts are marked by dashed lines. (**b**–**e**) SAD patterns from grains indicated as 1–3 and 5, respectively. The STEM-EDS results from the grains and regions annotated as 3–7 are presented in Table 6

Table 6 The Cu to Al concentration ratios, as measured by STEM-EDS from the regions noted in Fig. 10

	Cu (at.%, relative to Al) (%)
Grain 3	38 ± 0.6
Grain 4	38.6 ± 1.1
Grain 5	37 ± 0.6
Grain 6	40.6 ± 0.6
Region 7	76.5 ± 6

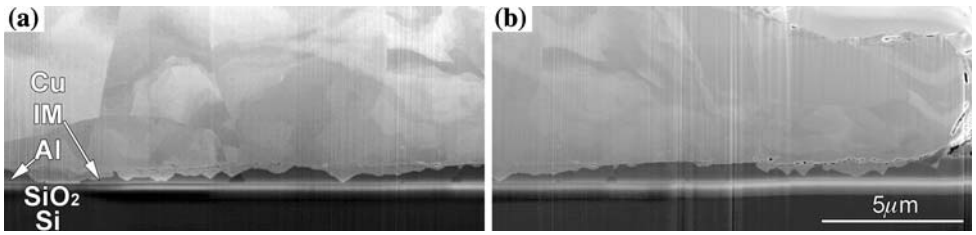

Fig. 11 SE HRSEM micrographs taken from (**a**) the center and (**b**) periphery of a copper wire-bond heat-treated for 200 h at 175 °C in argon. The scale bar is equivalent for both micrographs. A discontinuous intermetallic layer is detected

Specimens heat-treated in argon for 200 h at 175 °C

Figure 11 presents HRSEM micrographs taken from (a) the center and (b) the periphery of a bond heat-treated for 200 h in argon. The intermetallic coverage of the Al–Cu interface is not complete. Regions at the interface with no intermetallics can still be found. The intermetallics found at the bond periphery are less uniform than those found at the bond center. The intermetallics found at the bond center are more continuous. At several regions, the aluminum metallization was completely consumed by the intermetallics. Pores between the copper ball and the intermetallics located at the bond periphery can be detected. However, no pores were found between the intermetallics and the SiO_2 layer.

HRSEM micrographs, acquired from the center and the periphery of a bond heat-treated for 200 h in argon, are presented in Fig. 12. At the center of the bond, more continuous intermetallics, which are uniform in thickness, are visible (Fig. 12a). Two intermetallic layers with different contrasts can be distinguished. Singular pores found at the center of the bond are located at the interface between the regions labeled IM 1 and IM 2. At the bond periphery (Fig. 12b), a discontinuous void-line propagating from the bond edge was detected. The void-line does not intersect the pores found at the Cu–IM interface. Two intermetallic layers are also distinguishable. The pores found at the Cu–IM interface are located between copper and IM 2, and between the two intermetallic layers.

Figure 13 presents a BF STEM micrograph taken from the periphery of a specimen heat-treated for 200 h in argon. A discontinuous intermetallic layer was detected at the Al–Cu interface. A discontinuous void-line can be seen in regions of intermetallic growth. The composition of the larger intermetallic grains, noted on the micrograph as 4, 8, 9, and 11, was found by STEM-EDS to be close to the composition of Al_2Cu (within an error of 3 at.%). The smaller grains, adjacent to the copper ball, were found to contain a higher copper concentration. The SAD patterns, acquired from the large intermetallic grains (noted on the micrograph as 1, 2, and 4), confirmed the presence of the Al_2Cu phase. The smaller grain located adjacent to the copper ball (noted as 5 on the micrograph) and one larger grain (noted as 8 on the micrograph) were identified by SAD to be Al_4Cu_9. The intermetallic grain found at the Al–SiO_2 interface was identified to be Al_2Cu by STEM-EDS and SAD, while the two grains located above it were identified by STEM-EDS to be aluminum containing $\sim$1 wt.% Cu (Table 7).

Figure 14 presents a BF STEM micrograph acquired from the center of a bond heat-treated for 200 h in argon. A continuous intermetallic layer was detected. The large intermetallic grains are relatively uniform in size. Smaller intermetallic grains having a darker contrast are adjacent to the copper layer. The large intermetallic grains noted as 2–9 on the micrograph were sampled by STEM-EDS and found to contain 37–40 at.% Cu. Analysis of the SAD patterns from the large intermetallic grains, noted as 3 and 9 on the micrograph, confirmed the presence of Al_2Cu. Smaller intermetallic grains (noted as 1 and 10–13 on the micrograph) were found to contain larger amounts of copper, and were identified by SAD as the copper-rich Al_4Cu_9 phase (Fig. 14d–f) (Table 8).

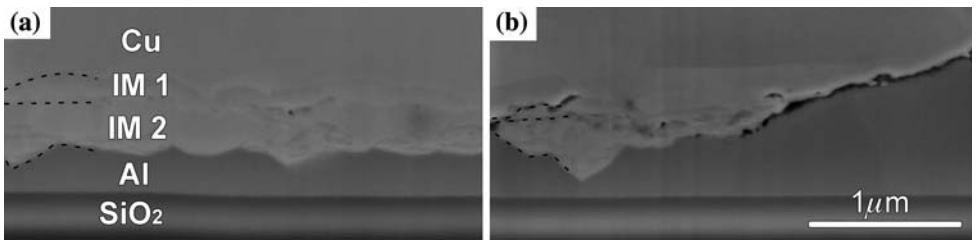

Fig. 12 SE HRSEM micrograph taken from (**a**) the center and (**b**) the periphery of a copper wire-bond heat-treated for 200 h at 175 °C in argon. Two intermetallic layers are detected and marked on the micrographs by dashed lines. The scale bar is equivalent for both micrographs

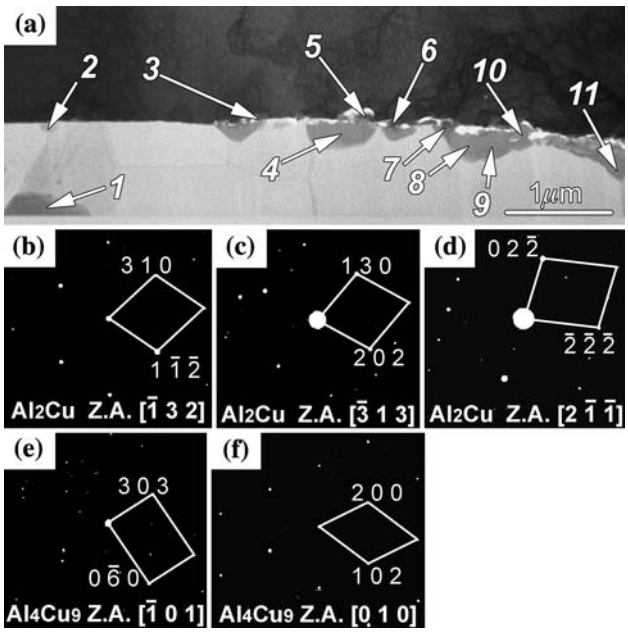

Fig. 13 (**a**) A BF STEM micrograph taken from the periphery of a wire-bond heat-treated at 175 °C for 200 h in argon. (**b**–**f**) SAD patterns from grains indicated as 1, 2, 4, 5, and 8, respectively. The STEM-EDS analysis results of the grains annotated as 1 and 3–11 are presented in Table 7

Table 7 The Cu to Al concentration ratios, as measured by STEM-EDS from the regions noted in Fig. 13

Grain	Cu (at.%, relative to Al) (%)
1	29.9 ± 0.5
3	62.2 ± 0.6
4	35.1 ± 0.6
5	56.9 ± 3.1
6	66.8 ± 2.8
7	56.9 ± 0.7
8	35.5 ± 0.6
9	34.4 ± 0.6
10	39 ± 0.6
11	37.6 ± 0.5

Microstructural and compositional evolution of the heat-treated Al–Cu wire bonds

The evolution of the microstructure and intermetallic composition of the Al–Cu wire-bond as a function of heat-treatment time (in argon) are schematically presented in Fig. 15. The length of the intermetallic layers was measured at the center of the bonds using STEM micrographs.

As noted in our previous report [2], discontinuous intermetallics were found in *as-bonded* specimens. The thickness of the intermetallic layer increases with heat-treatment time. Up to 200 h at 175 °C, the intermetallic layer remains discontinuous. The main intermetallics were found to be the Al_2Cu phase, while after 96 h at 175 °C, the Al_4Cu_9 intermetallic phase appears adjacent to the copper ball. Voids were found at the IM–Cu interface and between the two intermetallic layers. After 96 h at 175 °C, the Al layer was partially consumed by intermetallic growth. However, no voids were found at the Al_2Cu–SiO_2 interface.

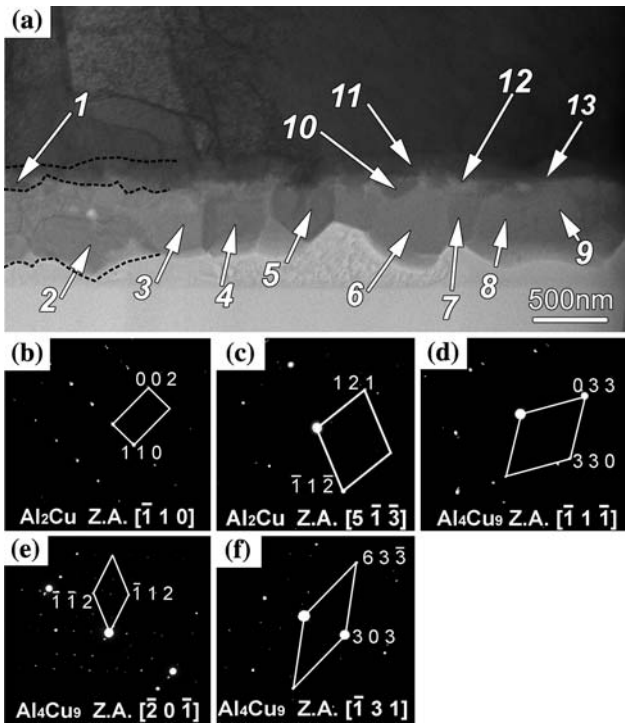

Fig. 14 A BF STEM micrograph taken from the center of a wire-bond heat-treated at 175 °C for 200 h in argon. Two intermetallic regions are marked by dashed lines. (**b**–**f**) SAD patterns from grains indicated as 3 and 9–12, respectively. The STEM-EDS results of the grains annotated as 1–10 and 13 are indicated in Table 8

Table 8 The Cu to Al concentration ratios, as measured by STEM-EDS from the regions noted in Fig. 14

Grain	Cu (at.%, relative to Al) (%)
1	69.6 ± 1.3
2	36.7 ± 0.5
3	38.4 ± 0.5
4	37.1 ± 0.5
5	40.2 ± 0.5
6	37.5 ± 0.4
7	38.3 ± 0.4
8	37.3 ± 0.4
9	38.2 ± 0.4
10	53.6 ± 0.5
13	76.4 ± 0.4

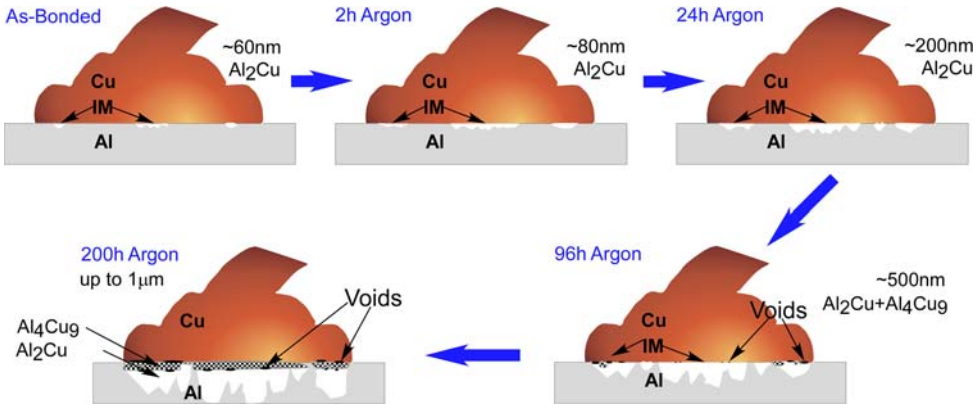

Fig. 15 Schematic representation of the intermetallic morphology and evolution at Al–Cu wire-bonds as a function of heat-treatment time

Discussion

For all of the examined specimens, including specimens that underwent heat-treatments of up to 200 h at 175 °C, intermetallic growth was discontinuous. The intermetallics grew mainly in regions of initial intermetallic formation; at the bond center and the bond periphery. This result leads to the assumption that the activation energy for intermetallic nucleation can only be attained during the wire-bonding process.

Al–Cu intermetallic composition

According to the Al–Cu phase diagram, five stable intermetallic phases can exist below 300 °C [18]. In the wire-bonded system studied in the current research, the main intermetallic phase found in the as-bonded and heat-treated specimens is Al_2Cu. In specimens heat-treated for 96 and 200 h, Al_4Cu_9 was detected adjacent to the copper wire. The Al_4Cu_9 phase first appeared at the bond periphery in specimens heat-treated for 96 h. This leads to the conclusion that one of the reasons for Al_4Cu_9 formation was the discontinuity of the Al_2Cu grains. Voids between the Al_2Cu grains inhibited their growth and may be responsible for the formation of Al_4Cu_9. However, the Al_4Cu_9 phase was also found at the center of wire bonds in regions without voids, which were heat-treated for 200 h (Fig. 14), proving that voids found adjacent to the Al_2Cu grains at the bond periphery were not the sole reason for Al_4Cu_9 formation.

It should be noted that the intermetallic composition measured by STEM-EDS can differ by as much as 15 at.% from the results obtained by SAD analysis (see Figs. 6, 9, 13, and 14). In the regions adjacent to the copper ball, STEM-EDS analysis usually showed a higher copper concentration than that measured by SAD. There are two main reasons for the differences in results from these two techniques:

1. The thickness of the investigated TEM specimen might be greater than the thickness of the investigated grain. Thus, the SAD pattern was obtained from a grain which is in a low-index zone-axis (Bragg conditions) while the total specimen thickness contributed to STEM-EDS results.
2. In order to receive a strong EDS signal from a specific region, the specimen holder was tilted by 15° towards the EDS detector. Figure 16 presents a schematic illustration of the STEM-EDS experimental setup. For the case of a specimen tilted towards the detector (Fig. 16b), the region from which the information was obtained was not uniformly distributed around the incident beam. The region located closer to the detector contributes more intensity than the region that is located far from the detector. In this study, to reduce the signal received from the TEM grid, the copper side of the specimen was always located closer to the EDS detector. In this way, the EDS detector received a stronger copper signal.

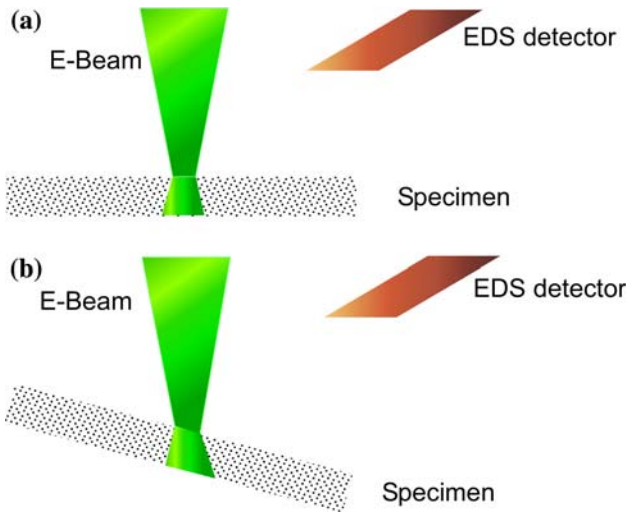

Fig. 16 Schematic representation of an experimental (**a**) untilted and (**b**) tilted STEM-EDS measurement setup

Al–Cu intermetallic morphology

Two types of voids were found at Al–Cu interfaces in heat-treated specimens; voids formed during the wire-bonding process and voids that evolved during heat-treatments. Voids formed during the bonding process were relatively large, continuous, and located at the bond periphery (see, e.g., Figs. 1 and 12). In general, these voids were not the source of bond failure (see, e.g., Fig. 12). Voids formed during the wire-bonding process were found mainly at the IM–Cu interface. These voids may shrink during heat-treatments [19, 20]. Voids that evolved during heat-treatments were usually found to be discontinuous, relatively small, detected mainly in specimens heat-treated for 96 and 200 h, and located at both the periphery and the center of the bonds. These voids were mainly found at Al_4Cu_9–Cu and at Al_4Cu_9–Al_2Cu interfaces.

To understand the processes that occur at the Al–Cu interface during intermetallic growth, atomic packing factors (APFs) of the Al_2Cu and Al_4Cu_9 intermetallics were calculated and compared to those of pure Al and Cu. The APFs of the intermetallic phases were calculated by dividing the total volume of atoms occupying the unit cell by the total volume of the unit cell (Eq. 1):

$$\mathrm{APF} = \frac{\Sigma N_{\mathrm{atoms}} V_{\mathrm{atoms}}}{V_{\mathrm{unit.cell}}}. \quad (1)$$

Table 9 presents APFs of pure metals and of the Al_2Cu and Al_4Cu_9 intermetallics. While the APF of Al_2Cu was very close to that of the pure metals, the APF of Al_4Cu_9 was 5% higher than that of Al_2Cu and of the pure metals. Therefore, voids formed at the Al_4Cu_9–Cu and Al_4Cu_9–Al_2Cu interfaces can be explained by volume reduction during Al_4Cu_9 formation.

Growth of the Al_2Cu Phase

Bonding of a single wire in the current experimental set-up took <0.2 s. The temperatures that evolve during ultrasonic activation at the Al–Cu interface are unknown, but may approach the melting points of the metals of interest [14]. In order to understand the grain growth of the Al–Cu intermetallics and to determine in which state intermetallic formation occurred, the grain growth of the Al_2Cu intermetallic phase was analyzed. Due to the lack of a uniform Al_4Cu_9 layer, the time-dependent growth of the Al_4Cu_9 phase was not analyzed.

The thickness of the Al_2Cu layer was measured at the center of as-bonded and heat-treated specimens (see the schematic drawing in Fig. 15). The specimens that were heat-treated for 200 h were not included in the analysis, since for those specimens it was difficult to distinguish between the Al_2Cu and the Al_4Cu_9 intermetallics. Figure 17 presents the square of the Al_2Cu intermetallic size as a function of heat-treatment time. The error bars represent the difference in thickness measured on different points of each intermetallic layer. Since there is a direct correlation between the square of the intermetallic thickness (x) and the heat-treatment time (t), the diffusion coefficient (D) of copper in Al_2Cu at 175 °C can be estimated from:

$$x = \sqrt{Dt}. \quad (2)$$

The activation energy (Q) for Al_2Cu formation was then estimated using the measured diffusion coefficient of copper in Al_2Cu at 175 °C (Eq. 3), where D and D_0 are the diffusion coefficients at the experimental temperature and at 0 K, respectively, and k_b is Boltzmann's constant.

$$D = D_0 \exp\left(-\frac{Q}{k_b T}\right). \quad (3)$$

The activation energy for Al_2Cu formation was found to be ~1.24 eV, which correlates with data acquired by Hamm and Vanderberg [21] for Al_2Cu formation via *bulk solid-state diffusion* in Al–Cu thin films at 157–220 °C (1.21–1.24 eV). A few intermetallic grains were found to grow toward the grain boundary between two aluminum grains in a manner similar to grain boundary diffusion (Figs. 1 grain 6, 7 grain 1, 9 grain 1 and more). Moreover, in two samples, copper was found to diffuse through the

Table 9 APFs of Al, Cu, and intermetallic phases found at the Al–Cu interfaces

Phase	APF
Al	0.74
Al_2Cu	0.739
Al_4Cu_9	0.776
Cu	0.74

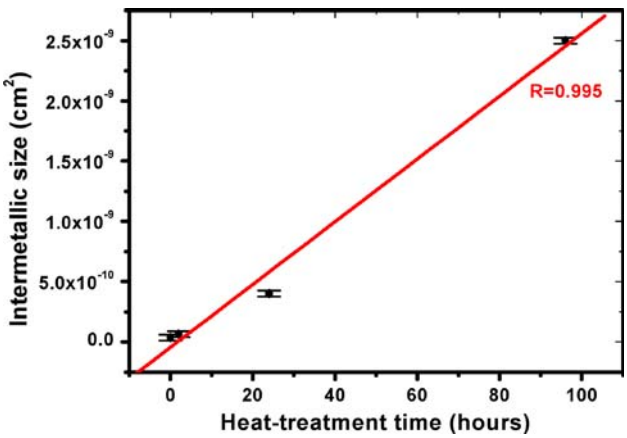

Fig. 17 The square of intermetallic size as a function of heat-treatment time. The solid line is a linear fit of the data

aluminum grain boundaries and intermetallic grains were created (see Figs. 1 and 13). However, these examples of grain boundary diffusion were singular, and for heat-treatments of up to 200 h had little influence on the Al_2Cu intermetallic layer thickness. Thus, the main diffusion mechanism observed in this system remains bulk solid-state diffusion.

Summary and conclusions

The purpose of this research was to understand the time-dependent behavior of Al–Cu wire bonds. To achieve this goal, Al–Cu intermetallic growth was studied at elevated temperatures. In order to receive maximum information regarding the studied processes, high resolution microscopy techniques were used. Specimens were prepared using a site-specific and relatively artifact-free technique (FIB), and morphological analysis of the specimens was conducted by HRSEM, FIB, and TEM. STEM-EDS and SAD were used for phase identification. The accuracy of STEM-EDS analysis in the current research was relatively poor. However, this technique enabled statistical sampling of the intermetallic grains. SAD analysis provided precise intermetallic phase identification and confirmed the results obtained by STEM-EDS.

The main intermetallic phase in the heat-treated specimens was found to be Al_2Cu. After longer heat-treatment times, Al_4Cu_9 was found. Al_2Cu grain growth occurred via solid-state diffusion. The growth of Al_2Cu at the bond periphery was partially inhibited by voids adjacent to the Al_2Cu grains, a phenomenon that was also responsible for enhanced Al_4Cu_9 growth at the bond periphery.

Two types of voids were found at the Al–Cu interface; discontinuous voids that were formed during the wire-bonding process, and pores that evolved during the heat-treatments. Voids that were formed during the wire-bonding process were usually located at the IM–Cu interfaces. These voids did not result in bond failure and partially closed during thermal annealing. Voids that formed during thermal annealing were found at interfaces between the intermetallics and copper, and at interfaces between the intermetallic grains, and were probably created by a mechanism of volume reduction during Al_4Cu_9 intermetallic formation. Almost no continuous void-lines were found in specimens heat-treated at 175 °C for up to 200 h. Thus, it can be stated that void formation in specimens heat-treated for 200 h was not a main source for bond failure.

No quantitative data regarding the reliability of heat-treated bonds was obtained in this research. In order to correlate between the intermetallic structure and the bond reliability, extensive mechanical and electrical tests of heat-treated specimens should be performed.

Acknowledgements The authors wish to thank A. Berner, Y. Kauffmann, and I. Popov for fruitful discussions. This research was partially supported by the Russell Berrie Nanotechnology Institute at the Technion.

References

1. Harman G (1997) Wire bonding in microelectronics materials, processes, reliability and yield. McGraw-Hill, New York
2. Drozdov M, Gur G, Atzmon Z, Kaplan WD (2008) J Mater Sci. doi:10.1007/s10853-008-2954-x
3. Brydson R, Bruley J, Mullejans H, Scheu C, Ruhle M (1995) Ultramicroscopy 59(1–4):81. doi:10.1016/0304-3991(95)00020-2
4. Sadan H, Kaplan WD (2006) J Mater Sci 41(16):5099. doi:10.1007/s10853-006-0437-5
5. Toyozawa K, Fujita K, Minamide S, Maeda T (1990) IEEE Trans Compon Hybr Manuf Technol 13(4):667. doi:10.1109/33.62577
6. Singh I Sr, On JY, Levine L Sr (2005) Proc Electron Compon Technol 55(1):843
7. Tan CW, Daud AR (2002) J Mater Sci Mater Electron 13(5):309. doi:10.1023/A:1015580227090
8. Murali S, Srikanth N, Vath CJ (2003) Mater Charact 50(1):39. doi:10.1016/S1044-5803(03)00102-5
9. Wulff FW, Breach CD, Saraswati SD, Dittmer KJ (2004) Proceedings of electronics packaging technology confernce, Singapore, 8–10 December, p 348
10. Onuki J, Koizumi M, Araki I (1987) IEEE Trans Compon Hybr Manuf Technol 10(4):550. doi:10.1109/TCHMT.1987.1134799
11. Ratchev P, Stoukatch S, Swinnen B (2006) Microelectron Reliab 46(8):1315. doi:10.1016/j.microrel.2005.11.002
12. Kim H-J, Lee JY, Paik K-W et al (2003) IEEE Trans Compon Packag Tech 26(2):367. doi:10.1109/TCAPT.2003.815121
13. Murali S, Srikanth N, Wong YM, Vath CJ (2007) J Mater Sci 42(2):615. doi:10.1007/s10853-006-1148-7
14. Karpel A, Gur G, Atzmon Z, Kaplan WD (2007) J Mater Sci 42(7):2334. doi:10.1007/s10853-007-1592-z
15. Karpel A, Gur G, Atzmon Z, Kaplan WD (2007) J Mater Sci 42(7):2347. doi:10.1007/s10853-007-1593-y
16. Murali S, Srikanth N, Vath CJ (2006) J Electron Packag 128(3):192. doi:10.1115/1.2229214
17. Thangadurai P, Lumelsky Y, Silverstein MS, Kaplan WD (2008) Mater Charact. doi:10.1016/j.matchar.2008.02.007
18. Murray JL (1985) Int Met Rev 30(5):211
19. Hill A, Wallach ER (1989) Acta Metall 37(9):2425. doi:10.1016/0001-6160(89)90040-0
20. Takahashi Y, Inoue K, Nishiguchi K (1993) Acta Metall Mater 41(11):3077. doi:10.1016/0956-7151(93)90036-R
21. Hamm RA, Vandenberg JM (1984) J Appl Phys 56(2):293. doi:10.1063/1.333960